scientific reports

Check for updates

OPEN

Health status assessment of pump station units based on spatio-temporal fusion and uncertainty information

Panpan Qiu, Jianzhuo Yan, Hongxia Xu & Yongchuan Yu✉

An effective health status assessment (HSA) for pump station units (PSUs) is crucial for accurately determining their real status and providing technical support for safe operational decisions. Due to the limitations of existing data-driven HSA methods, which primarily focus on the temporal dependencies of monitoring signals and fail to explore the complex interconnections among signals comprehensively. Moreover, when constructing performance degradation indices based on linear differences, these methods do not effectively integrate heterogeneous signals, resulting in an incomplete and inaccurate assessment of the overall system degradation. This paper proposes a real-time comprehensive HSA method for PSUs based on multi-source heterogeneous uncertainty information. Initially, a health benchmark model (HBM) is built using CrossGNN, which possesses cross-scale and cross-variable interaction capabilities, to precisely capture the temporal dependencies and dynamic relationships among variables in monitoring signals. Subsequently, key measurement points that reflect the operational status of the PSUs are identified through correlation analysis to establish multi-source evaluation indices. Then, considering the uncertainty in signal changes, a novel health degradation index (HDI) is developed using Mahalanobis distance (MD) and the Gaussian Cloud Model (GCM) to analyze changes in unit status. Furthermore, a weighting calculation method based on the non-dominated sorting genetic algorithm (NSGA-II) is proposed to establish a real-time comprehensive health index (RCHDI) for a thorough assessment of PSUs status. Finally, the effectiveness of the proposed method is validated through a case study using data from a pump station in the South-to-North Water Diversion Project in China. The results show that, compared to other studies, the proposed method significantly improves the stability and smoothness of the state assessment curve, with increases of 21.5% and 47.1% respectively, providing a new perspective for comprehensively assessing the health status of PSUs.V

Keywords Pump station units, Health status assessment, Spatio-temporal Interaction, Weight optimization, Comprehensive health degradation index

Introduction.

Pump station engineering is pivotal within hydraulic engineering, serving essential roles such as flood control and drainage, and thereby demanding high operational safety standards[1]. The machinery units, central to pump station operations, are crucial for the stable functioning of water management systems[2]. Given this context, prioritizing the health and efficiency of PSUs is imperative[3]. Currently, maintenance of PSUs primarily relies on post-failure repairs and scheduled preventative measures. This approach leads to simultaneous under-maintenance and over-maintenance, escalating safety risks and maintenance costs[4]. To address these issues, a shift from reactive to proactive maintenance is necessary[5]. Accordingly, the assessment of PSUs health status has emerged as a significant research area[6], where effective Health Status Assessments (HSAs) can facilitate the development of reliable maintenance schedules, thus preempting potential failures.

Health assessment methods for equipment primarily fall into three categories: physics-based, knowledge-driven, and data-driven approaches. The mechanical structure of PSUs is complex, and the mechanisms of degradation in complex environments have not been fully revealed. Moreover, the degradation of key components is intricate, with interdependencies that complicate accurate model development[7]. Knowledge-

School of Information and Communication Engineering, Beijing University of Technology, Beijing 100124, China. ✉email: yuyongchuan@bjut.edu.cn

driven models rely on expert experience to map degradation characteristics to health states but are susceptible to subjective biases. With advancements in sensor technology, PSUs are equipped with numerous sensors to monitor operational status in real-time[8], making data-driven methods increasingly popular. Without the involvement of human experience, automatic feature extraction and dimensionality reduction are performed on operational data to construct a nonlinear relationship between degraded features and health status, achieving modeling of device performance degradation[9].

HSA using data-driven methods typically involves three steps: First, a HBM is constructed based on monitoring data collected during the unit's healthy state. Next, this HBM is used to predict real-time monitoring signals. Finally, a HDI curve is constructed from the differences between predicted and actual signals to characterize the equipment's degradation process[10–13]. Consequently, the HBM's fitting ability in complex conditions and the scientific rigor in constructing the HDI are crucial for the effectiveness of HSA[14]. An et al. employed Radial Basis Function Neural Networks and grey theory to map the relationships between head, power, and vibration signals[15]. Fu and colleagues developed a model using Aggregated Ensemble Empirical Mode Decomposition and Optimized Support Vector Regression (SVR) to fit the relationship between the guide vane and PSUs vibration signals[16]. However, previous studies often focused solely on single-component monitoring data, neglecting the impact of various components on overall health, which can lead to the loss of critical state information and incomplete health assessments of units[17]. Consequently, recent research has explored integrating multi-source monitoring data. Shan et al.[7] utilized a combined multi-objective optimization backpropagation neural network (BPNN) to learn the relationships between multidimensional monitoring parameters and multiple vibration signals; Zhang et al.[14] developed a deep HBM based on a multi-head self-attention network (MSNN) to study the functional relationships between multidimensional monitoring parameters and multiple vibration signals. These studies considered multidimensional monitoring indicators but focused only on their temporal characteristics, overlooking internal spatial dependencies, and the inherent characteristics and dynamic changes among indicators, making simple averaging insufficient to accurately reflect the degradation state of the PSUs. Moreover, in constructing the HDI, many models have not adequately considered the overall distribution and uncertainty of data. For instance, Ye et al.[18] processed monitoring data using Long Short-Term Memory networks combined with autoencoder technology to generate reconstruction errors for calculating HI, but did not address the uncertainty in data distribution. Additionally, while Duan et al.[19] considered uncertainties by fitting the probability density distribution of monitoring data using Gaussian Mixture Models (GMM) to construct HI, the choice of model parameters and the comprehensiveness of data distribution remain challenging.

Despite the merits of existing methods, they still present several limitations: (1) When constructing models from multidimensional monitoring data, only the temporal characteristics of parameters are considered, ignoring the complex spatial dependencies formed by inter-variable connections. This oversight limits the model's ability to fully learn from the interactive multidimensional data. Additionally, real-world operational anomalies, human interference, and equipment malfunctions introduce noise that degrades data quality, resulting in reduced accuracy of the HBM and unstable assessment outcomes. (2) Given the variability of PSUs operating conditions, learning solely from signal amplitude overlooks the randomness and uncertainty of monitoring signals. When constructing the HDI based on deviations, the overall distribution of data is not considered, leading to significant errors in the HDI. (3) The use of a comprehensive evaluation index, RCHDI, to assess the overall health of the unit is complicated by the inherent characteristics and dynamic changes of different indicators, which vary in real-time. Simple averaging methods fail to accurately depict the degradation state of the PSUs.

To more accurately and reliably assess and predict the health status of PSUs, this study proposes a health state assessment method for PSUs based on the integration of spatiotemporal and uncertainty information. The proposed method aims to overcome the three aforementioned drawbacks. First, it establishes an HBM by mining the potential spatiotemporal dependencies in multidimensional monitoring data of pump station units across scales and variables. Second, it introduces a HDI construction method based on MD and GCM. Finally, it employs a dynamic multi-objective optimization algorithm for weighting calculations combined with a sliding window mechanism to dynamically update weights, ultimately yielding an RCHDI that thoroughly characterizes the health state of the unit. The main contributions are summarized as follows:

1) Construction of multi-scale time series with varying noise levels using cross-scale interactive GNN to capture clearer trends and weaker noise time scales, and cross-variable interactive GNN to capture dynamic correlations between different variables. This improves the robustness of the Health Benchmark Model to industrial noise and addresses the complex spatiotemporal dependencies in multidimensional monitoring data that existing methods fail to handle adequately.

2) Introduction of an HDI construction method based on MD-GCM that considers the uncertainty of actual industrial monitoring signals. The MD incorporates the intrinsic structure and distribution characteristics of data, enhancing the sensitivity of the HDI to changes in the health state of the unit.

3) Application of a dynamic multi-objective optimization algorithm to determine indicator weights for the RCHDI, eliminating the need for manual criteria setting or reliance on expert experience. This reveals the intrinsic properties and real-time dynamic changes of each HDI, thereby comprehensively characterizing the variations in the unit's health state.

The remainder of this paper is organized as follows: Sect. 2 provides a brief introduction to the relevant foundational knowledge. Subsequently, Sect. 3 elaborates in detail on the framework of the proposed technique. Section 4 discusses the engineering applications and comparative analysis of the method. Finally, the study is discussed and summarized in Sects. 5 and 6, respectively.

Background knowledge

Graph neural network

Graph Neural Networks (GNNs) are a category of deep learning models specifically designed to handle non-Euclidean graph structure data. These models utilize the topology of graphs to learn meaningful representations of nodes and edges. Through a message-passing mechanism, they effectively propagate and aggregate information along the edges of the input graph, enabling the acquisition of expressive node representations[20–22]. The operation of GNNs primarily includes three fundamental steps: message passing, information aggregation, and node updating.

First, at the $l-\mathrm{th}$ layer of the graph, for each edge (i,j), GNN computes the message $m_{ij}^{l}=Message\left(h_{i}^{l-1},h_{j}^{l-1}\right)$ using a predefined message function, where h_{i}^{l-1} and h_{j}^{l-1} respectively represent the states of nodes i and j from the previous layer, simulating the process of information transfer between nodes. Next, for each node i, GNN aggregates the information transmitted by its neighborhood $N(i)$ through the aggregation function Aggregation $m_{i}^{l}=Aggregation\left(\left\{m_{ij}^{l}|j\in N(i)\right\}\right)$ to form a comprehensive message representation. Finally, GNN updates the vector representation of each node i using the update function Update $h_{i}^{l}=Update\left(m_{i}^{l},h_{i}^{l-1}\right)$, which takes the aggregated message and the current node's representation as inputs to update the representation of each node. The final node $z_i=h_i^l$ embedding representation is $z_i=h_i^l$, which is the hidden representation obtained from the last layer of GNN. After obtaining the node embeddings, GNN uses the READOUT function to learn the representation of the entire graph $h_G=READOUT\left(\{z_i|i\in G\}\right)$, where h_G is the representation of graph G.

Gaussian cloud model

As system complexity increases, the issue of uncertainty becomes more prevalent[23]. In response to this, researchers have proposed using rough set theory and fuzzy set theory to address this problem. Rough set theory expresses the uncertainty of things through upper and lower approximations, while fuzzy set theory introduces the concept of membership degrees to describe the degree of uncertainty in objects. However, these methods often rely on expert experience or prior knowledge when determining membership functions and degrees, leading to significant subjectivity and difficulty in accurately reflecting real-world issues[24]. In contrast, the GCM[25,26], an implementation of cloud modeling, quantifies the digital characteristics of a qualitative concept through three parameters: expectation (Ex), entropy (En), and hyper-entropy (He). This model integrates fuzziness and randomness, achieving a mapping between qualitative and quantitative aspects, and scientifically handles uncertainty issues without being constrained by expert subjective judgments.

The definition is as follows: Assume $C(Ex,En,He)$ is a qualitative concept on the quantitative domain U, and a single random instantiation $x\,(x\in U)$ satisfies $x\sim N(Ex,En')$, where Ex is the expected value and En' is the variance of a Gaussian distribution; simultaneously, it satisfies $En'\sim N\left(En,He^{2}\right)$, where En is the expected value and He^2 is the variance for En'. The association degree the association degree $\mu_c(x)\in[0,1]$ of x with respect to C satisfies:

$$\mu_c(x)=e^{-(x-Ex)^2/2\left(En'^2\right)} \tag{1}$$

The distribution $\mu_c(x)$ in the domain U is called a membership cloud, which can be characterized by the GCM, and each (x,μ) is referred to as a cloud droplet. Here, the expected value Ex is the center of the cloud droplets' spatial distribution in the domain and represents the point value that best characterizes concepts such as equipment status levels; the entropy En measures the uncertainty of the status level concept, determined by the degree of dispersion and ambiguity; the hyper-entropy He represents the uncertainty of the entropy, corresponding to the thickness of the cloud droplets.

NSGA-II algorithm

The Non-dominated Sorting Genetic Algorithm (NSGA) is a genetic algorithm based on the concept of Pareto optimization, facilitating decision-makers to make choices based on different preferences [27]. The NSGA-II algorithm has been proven to effectively solve complex multi-objective problems across various technical fields. For instance, in the field of structural engineering, the algorithm was applied to optimize the vibration control system of a 20-story steel structure by adjusting actuator placements and tuning, which not only significantly enhanced system performance but also reduced computational costs and accelerated convergence to the Pareto front[28]. In the realm of energy management, NSGA-II was used for a multi-objective optimization model targeting low-carbon, economical, and safe operation of Ultra-High Voltage Direct Current (UHVDC) systems. It outperformed other mainstream algorithms by significantly reducing carbon losses and trading costs, achieved through improved population initialization and crowding calculation strategies[29]. Additionally, in the optimization of battery thermal management systems, NSGA-II effectively lowered the highest system temperatures, temperature variance, and pressure drops by adjusting the battery spacing, cooling tube diameter, and inlet velocity, thus enhancing the cooling efficiency and economic viability of the system[30].

The widespread adoption of the NSGA-II algorithm in these complex multi-objective problems is primarily due to its effective balance between solution diversity and quality. This algorithm maintains population diversity through fast non-dominated sorting and crowding distance calculations, ensuring that the search process covers a broad area of the solution space. Moreover, NSGA-II elitism strategy ensures that superior solutions are not lost during the evolutionary process, thus enhancing the algorithm's convergence speed and the quality of optimized solutions. This effectively improves the algorithm's computational speed and robustness, converging to high-quality solutions that meet both optimization goals and constraints[31]. The specific steps of NSGA-II are [32,33]:

(1) Initialization randomly generates P with population size N, and set the evolutionary generation $GEN = 1$.
(2) Determine whether the first generation subpopulation has been generated. and add 1 to the number of evolutionary generations if it has been generated. Otherwise, the offspring Q_t of size N is generated by selection, crossover, and mutation, and the parent P_t is combined with the offspring Q_t to generate a population size R_t of $2N$.
(3) Fast non-dominated sorting. Non-dominated sorting is performed on R_t to obtain the non-dominated hierarchy $(F_1, F_2, \ldots, F_n)$. Then, put the members in the non-dominated layers F_1 to F_n into S, in order.
(4) If the number in S, is equal to N, there is no need to perform the following operation, directly $P_t + 1 = S_t$, and repeat steps (2) and (3). If the number in S_t is greater than N, the crowding distance should be calculated.
(5) Combining the parent population $P_t$and offspring population Q_t, a population $R_t = P_t \cup Q_t$of size $2N$ can be obtained, as shown in the Fig. 1. For population R_t, the nondominated layers are sorted in ascending order by the rank number after the nondominated sorting. The individuals in each layer are sorted in descending order by crowding distance. Then, the first N individuals are selected to form the new parent population $P_t + 1$.
(6) Finally, repeat steps (3) to (5) until the algorithm runs to the maximum number of iterations.

HCA experimental method

This paper proposes a health assessment method for PSUs based on multi-objective dynamic optimization of comprehensive health degradation indices: considering multi-variable spatio-temporal fusion and uncertainty distribution.

Figure 2 describes the method flow framework. First, to address the issue of insufficient mining of spatio-temporal dependencies in multidimensional monitoring data, an HBM based on cross-scale and cross-variable interactive graph neural networks is established; secondly, considering the randomness of monitoring signal changes and distribution differences, the MD-GCM is used to construct a HDI from multi-source monitoring indicators; finally, to comprehensively characterize the health status of the unit in real time, a dynamic multi-objective optimization algorithm is used to integrate multiple HDIs to generate the RCHDI.

HBM based on interactive GNN

This method aims to accurately mine spatio-temporal dependencies by overcoming noise interference in multidimensional time-series data. Initially, multisensor monitoring data, influenced by internal sensor correlations, exhibit complex nonlinear coupling and heterogeneous distribution of samples. Furthermore, various monitoring signals in the PSUs, such as voltage, current, and temperature, dynamically interact and collectively impact the operational state of the pump station units. Additionally, noise in sensor data increases the complexity of predictions. Therefore, effectively handling unexpected noise in multidimensional monitoring data of the pump station and accurately capturing sequence dependencies and dynamic correlations are key to constructing the HBM. The process of constructing the health model for the pump station units is shown in Fig. 3.

Adaptive multi-scale recognizer

Design an adaptive multi-scale recognizer using Fast Fourier Transform (FFT)[34]to extract key frequency components from multidimensional time series. By analyzing the average amplitude of these frequencies, identify the periodic variations in the data, and based on this, reconstruct time series representing different noise levels.

$$\widehat{A}(x) = \frac{1}{D}\sum_{d=1}^{D}\sqrt{(F(x)_d)^2 + (F(x)_d)^{*2}} \tag{2}$$

Here, $F(x)_d$ represents the d-th complex result of the signal x after the FFT transformation, $(\cdot)^*$denotes the complex conjugate. The sum of the squares of the real and imaginary parts is computed for each frequency component. Following this, the square root is taken to derive the amplitude, which is then averaged across all D amplitudes.

Select the top S frequencies with the highest amplitudes $\{f_1, f_2, \ldots, f_s\}$, calculating their respective lengths $\{p_1, p_2, \ldots, p_s\} = \{\frac{L}{f_1}, \frac{L}{f_2}, \ldots, \frac{L}{f_S}\}$, thus obtaining time series of S different scales.

$$X_s = AvgPool(X)_{kernel=stride=p_s} \tag{3}$$

Then, perform average pooling on each time series to capture sequence features from coarse to fine scales. Concatenate all scale time series to obtain $X' \in R^{L' \times D}$. After an expansive transformation to $X' \in R^{L' \times D \times C}$, input into the cross-scale interaction module.

Cross-scale interaction

Based on the scale features extracted in Sect. 3.1.1, initialize and configure a cross-scale temporal correlation graph. Each node in the graph represents different time points processed by the adaptive multi-scale recognizer. By analyzing the periodic characteristics of the nodes and selecting neighbors based on the correlations between them, construct a cross-scale graph[35]. Additionally, consider the temporal sequence to ensure that nodes are connected both to scale-related neighbors and to immediately adjacent nodes in time.

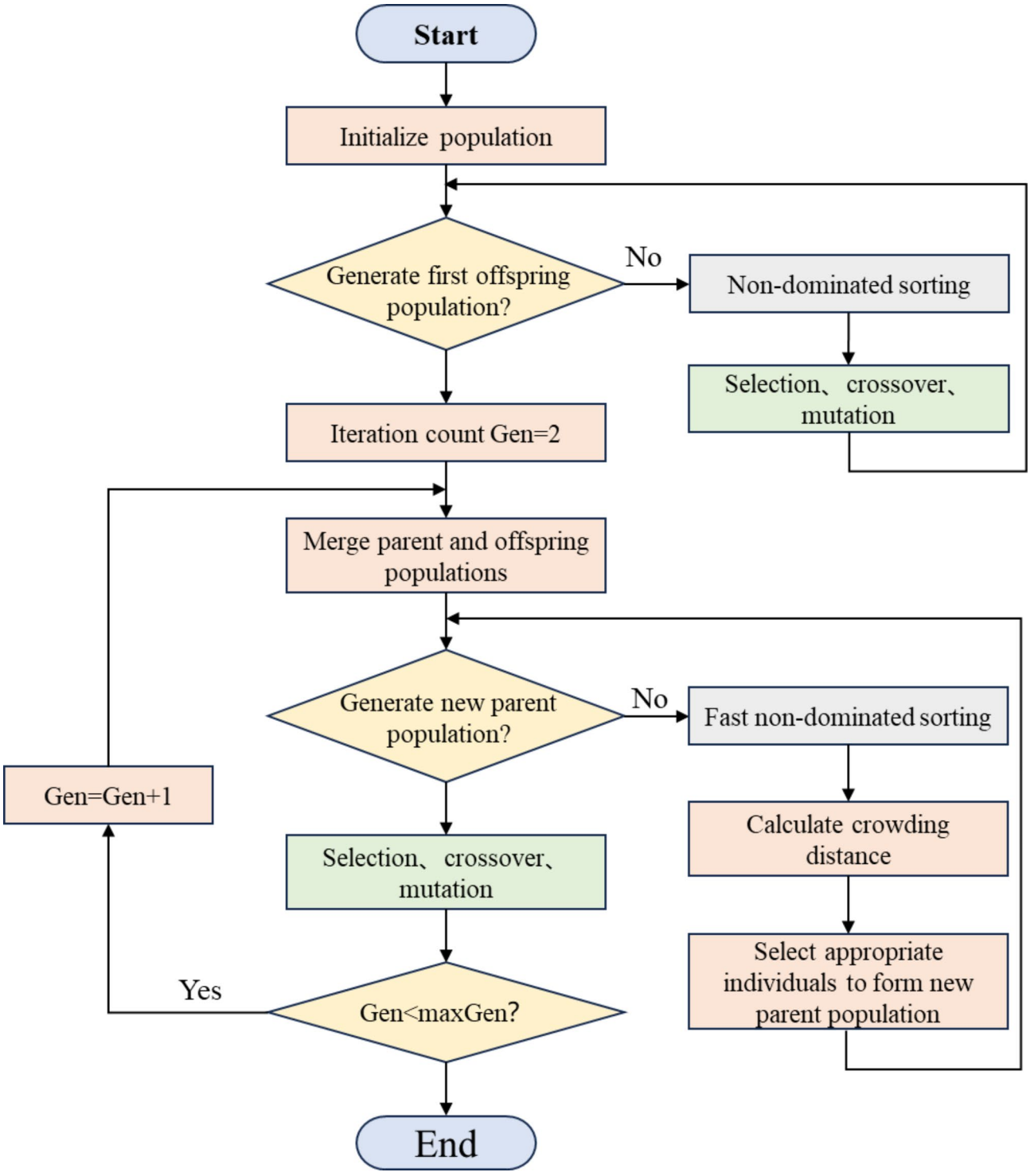

Fig. 1. NSGA-II procedure.

A cross-scale graph in the time dimension is represented as $G^{scale} = (V^{scale}, E^{scale})$, with nodes denoted by $V_{scale} = V_1^{scale}, V_2^{scale}, \ldots, V_{L'}^{scale}$. To reduce the impact of noise on association weights, two learnable vectors, vec_1^{scale} and vec_2^{scale} are used to initialize the relationship matrix between time nodes through the outer product form.

In constructing a cross-scale temporal correlation graph, a neighbor selection strategy based on the periodic characteristics of each time node is employed. The most strongly associated nodes from all possible neighbors are chosen to ensure that the connections in the graph accurately reflect the actual correlations between nodes.

$$N_s^{scale}\left(V_i^{scale}\right) = argTop - k_s\left(E_s^{scale}\left(V_i^{scale}\right)\right) \tag{4}$$

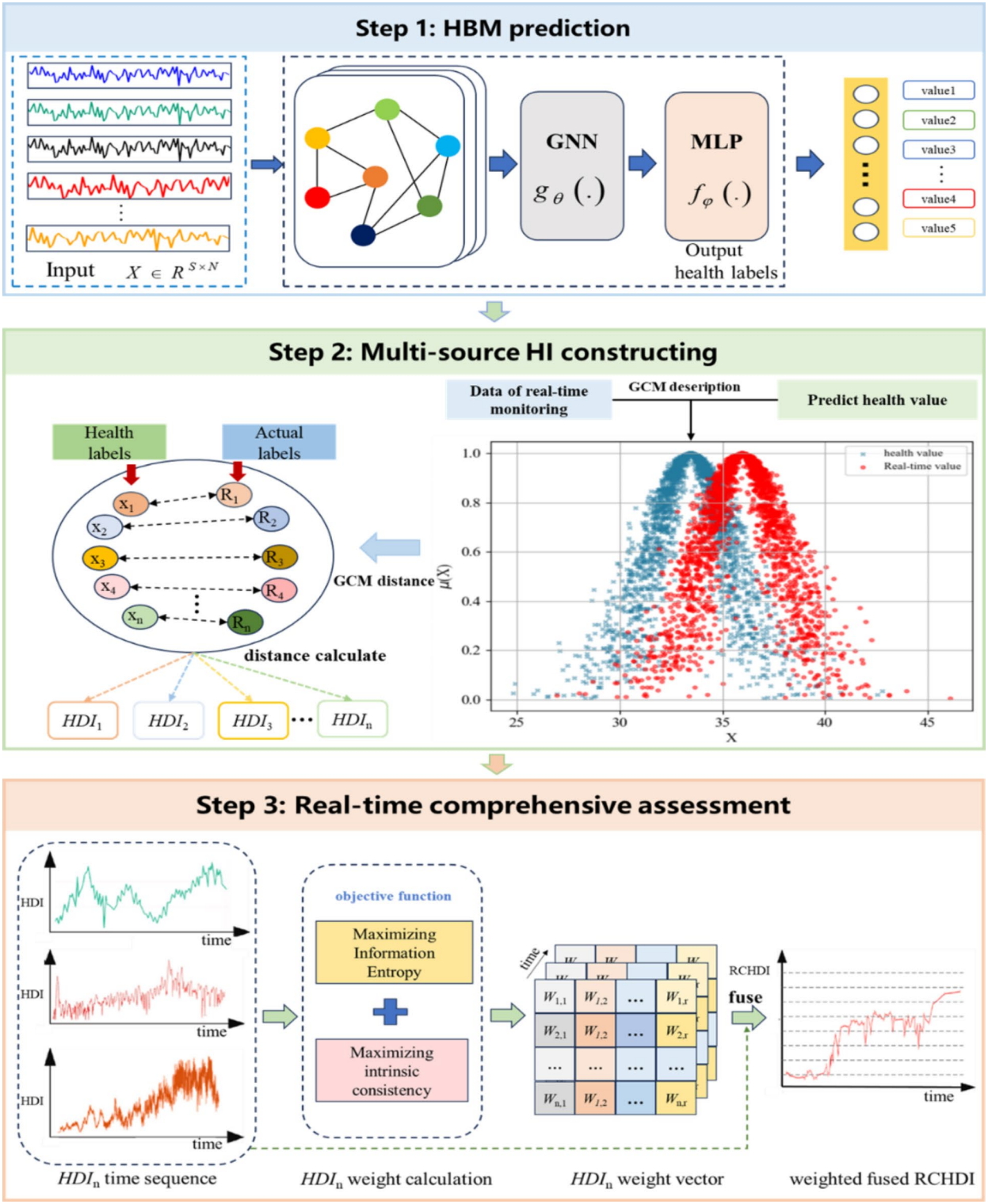

Fig. 2. Framework of the proposed HSA method.

Here, $argTop-k_s(\cdot)$ represents the operation of extracting the top k nodes with the highest relevance weights, and $E_s^{scale}\left(V_i^{scale}\right) \in R^{L(s)}$ denotes the relevance weight of the time node V_i^{scale} at scale s.

For each time node V_i^{scale}, in addition to selecting neighbors based on scale sensitivity, it is also necessary to consider the temporal order of the nodes to ensure connections are maintained with the immediately preceding and following nodes:

$$N^{trend}\left(V_i^{scale}\right) = \left\{V_i^{scale} \middle| |i-j| \leq 1, scale\left(V_i^{scale}\right) = scale\left(V_j^{scale}\right)\right\} \quad (5)$$

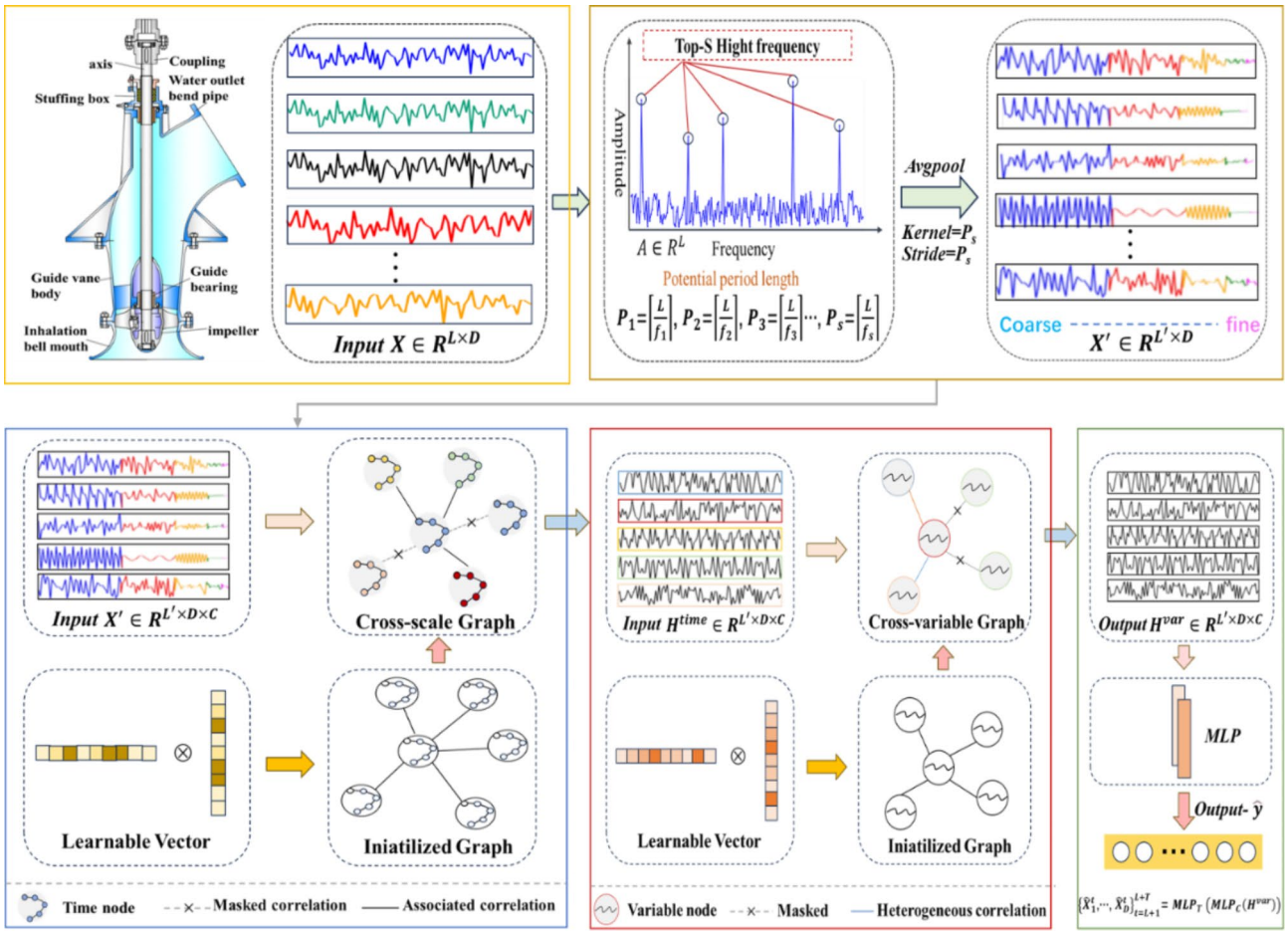

Fig. 3. PSUs HBM construction process.

Here, $scale\,(\cdot)$denotes the scale of a time node. The trend neighbor set of the time node V_i^{scale} consists of its immediate adjacent time nodes $(i, e., |i-j| \leq 1)$, where $|i-j| \leq 1$ ensures that only temporally adjacent nodes are selected, i.e., the previous and next time points.

In the cross-scale temporal correlation graph, each time node V_i^{scale}has a neighborhood consisting of scale-sensitive neighbors $N^{scale}(V_i)$ and trend neighbors $N^{trend}(V_i)$. These combined neighborhoods update the relevance weight matrix E^{scale} to reflect the connections between nodes. Information propagation is executed within this graph using GNN, where N stacked layers output the normalized time node features $H_{\cdot\cdot\cdot}^{t,N}$.

Cross-variable interaction

This module leverages the temporal node features obtained from the cross-scale interactions described in Sect. 3.1.2 to integrate multi-time-scale information, supporting deep interactive analysis between variables. Here, variables act as graph nodes, and relationships and information transfer between nodes are defined through GNN. Homogeneous and heterogeneous neighbors, as well as normalized weights, are set to precisely capture the complex dynamics between variables.

The cross-variable graph is denoted as $G^{var} = (V^{var}, E^{var})$, and $E^{var}$is initialized by generating two latent vectors $vec_1^{var}$and vec_2^{var}:

$$E^{var} = Softmax\left(ReLU\left(vec_1^{var} \times vec_2^{var}\right)\right) \tag{6}$$

Decomposehomogeneousandheterogeneousnodesets,selectthe K_+^{var}nodes $N_+^{var}(V_i) = Top - K_+^{var}\left(E^{var}(V_i)\right)$ with the strongest relevance to each variable node V_i^{var}as homogeneous (positive) neighbors, and choose the K_-^{var}nodes $N_-^{var}(V_i) = Bottom - K_-^{var}\left(E^{var}(V_i)\right)$ with the weakest relevance as heterogeneous (negative) neighbors.

For each variable node the V_i^{var}weights of its homogeneous and heterogeneous edges are normalized separately. Subsequently, the weights are updated to construct a cross-variable graph with distinct homogeneous and heterogeneous edges.

Cross-variable interactions are facilitated through the propagation of information on the cross-variable graph using a GNN. Each variable node's feature update incorporates the influence of its positive and negative

neighbors. The propagation process involves stacking Nlayers, ultimately outputting the normalized variable features $H_{:,i}^{var,N}$.

Multistep Prediction: The output features from the cross-variable interaction module are fed into two multilayer perceptrons (MLPs). The first MLP is used to map the time dimension of the features from T to 1, while the second MLP maps the time dimension from the historical input sequence length $L\prime$ to the target output sequence length.

$$\{\widehat{X}_1^t, \ldots, \widehat{X}_D^t\}_{t=L+1}^{L+T} = \mathrm{MLP_T?MLP_C}\,(H^{var})? \tag{7}$$

In the formula, D is the number of variables, L is the length of the input sequence, and T is the prediction step size.

Health degradation index construction

Using GCM, the amplitude variations and uncertainty information of monitoring signals are quantified, revealing the randomness and uncertainty of signal changes. Additionally, to minimize the impact of signal distribution differences on the accuracy of distance measurements, the deviation between the real-time operational state and the healthy operational state GCMs is calculated using MD to construct the HDI. This approach avoids the influence of model hyperparameters and enhances the sensitivity of the HDI to changes in the PSUs health status.

GCM modeling process

In the process of GCM modeling, the key to quantifying the dynamic changes of signals lies in understanding the interaction of signal components: amplitude, phase, and frequency. By defining the base component (BCG), we can effectively analyze how these components interact within the composite component $C\,(Ex, En, He)$, where Ex、 En、 He are the signal's amplitude, phase, and frequency respectively. Furthermore, by defining the frequency composite component (FCG) as (Ex, En, He), we establish a comprehensive description of the interaction, facilitating the comparison and differentiation between GCM1 and GCM2.

The GCM modeling process of PSUs vibration is shown in Fig. 4: (1) Convert the input quantitative sample value x_i into numerical features Ex, En, He; (2) Generate a normal random number $En\prime$ with an expected

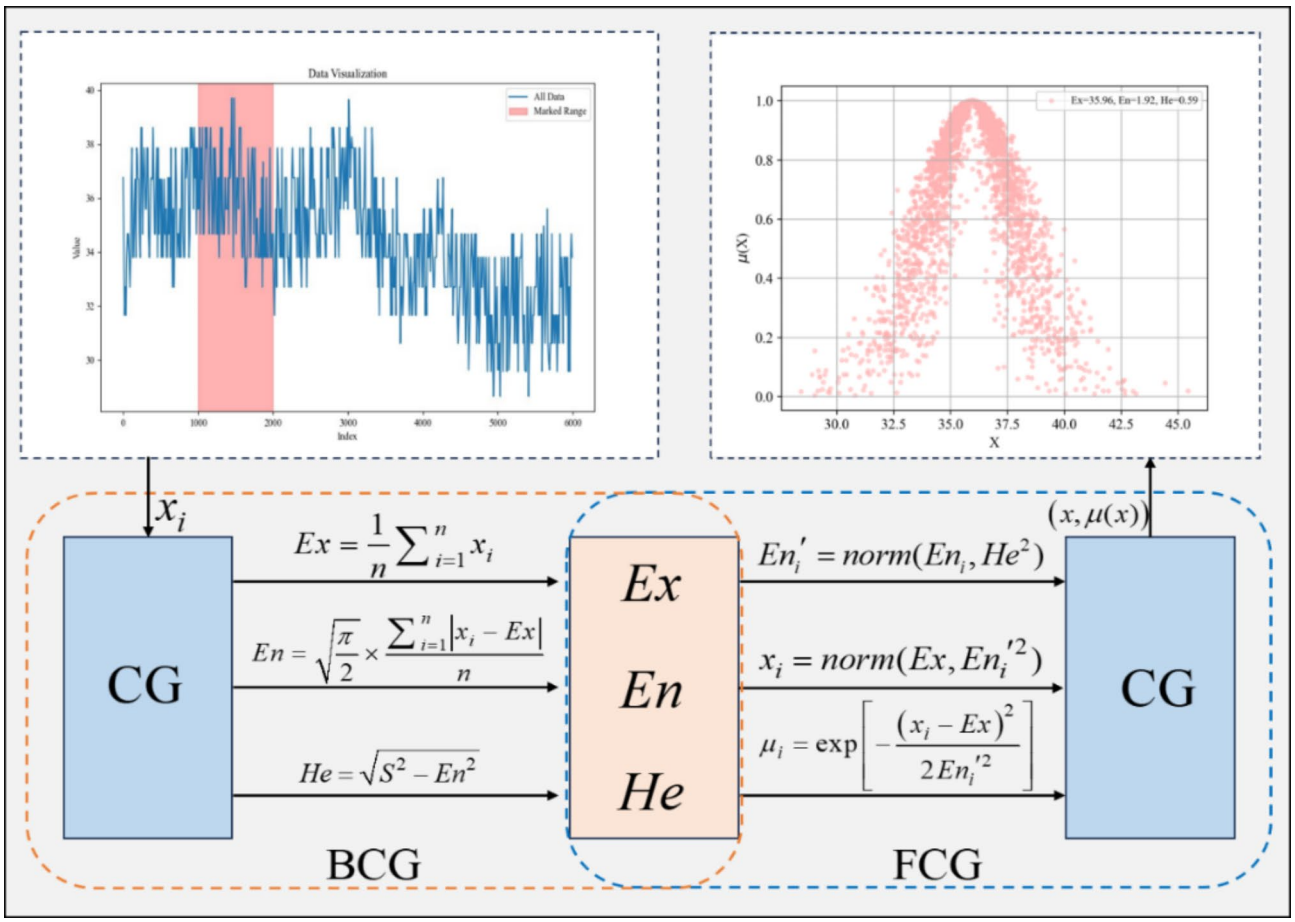

Fig. 4. GCM modeling process of PSUs vibration signals.

value of En and a standard deviation of He; (3) Generate a normal random number x_i with an expected value of Ex and a standard deviation of $En\prime$; (4) Obtain the degree of certainty that x belongs to qualitative concept C based on the formula $\mu_i = exp\left[-\frac{(x_i-Ex)^2}{2En_i'^2}\right]$; (5) Repeat the above calculation process N times to generate a cloud with N cloud droplets, N taken 3000 times.

To demonstrate the impact of these three factors on GCM, the qualitative idea is that the vibration of the pumping station unit is approximately $12.77\mu\, m$, represented by a Gaussian cloud as $C\,(Ex, En, He) = (12.77,1.74,0.28)$, as shown in Fig. 5 (a). The x-axis in the figure represents the value of cloud droplets, while the y-axis represents the degree to which cloud droplets belong to qualitative concepts. From Fig. 5b-d, it can be seen that Ex affects the central axis of the cloud, En changes the width of the cloud, and He affects the thickness of the cloud.

Building HDI based on MD-GCM

The deviation between the theoretical health status signal and the measured signal indicates the difference between the actual and baseline health status of the PSUs, providing a basis for constructing the HDI. Although directly comparing differences between two signals is a conventional method widely used in one-dimensional linear data[4], this approach has limited effectiveness in handling complex multi-source heterogeneous signals. To address this issue, multi-dimensional distance measurement methods such as Euclidean distance[36] and cosine distance [37] have been used to quantify signal differences. In more complex evaluations using cloud models, it is also necessary to analyze the interaction and statistical dependence of characteristic values in addition to considering the direct differences in model characteristic values. The MD can improve the sensitivity of the HDI to changes in unit health by considering the correlations and statistical characteristics of these values[38].

Using MD calculate the deviation between the real-time monitored GCM1 and the health-predicted GCM2. Each GCM has three numerical characteristics (Ex, En, He). Assuming that GCM1 (Ex_i, En_i, He_i) and GCM2 (Ex_j, En_j, He_j) are mapped into a three-dimensional space, the distance $diatance\,(I|J)$ between the two points would be:

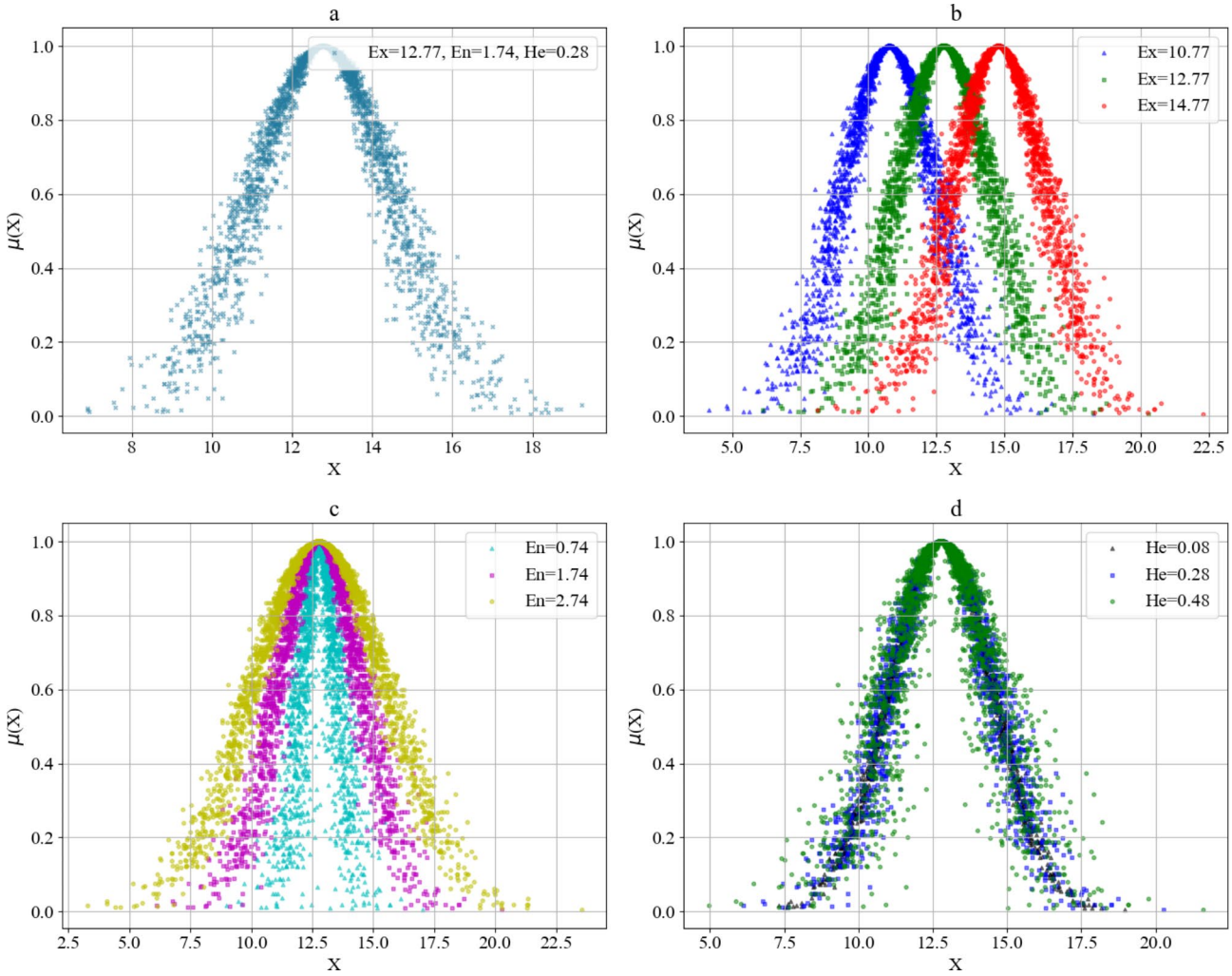

Fig. 5. Examples of GCM and its shape under different numerical characteristics. (**a**) Examples of GCM; (**b**) GCM has different Ex; (**c**) GCM has different En; (**d**) GCM has different *He*

$$D_{ij} = \sqrt{(I-J)^T S^{-1} (I-J)} \tag{8}$$

Here, vectors $I = (Ex_i, En_i, He_i)$ and $J = (Ex_j, En_j, He_j)$, while matrix S^{-1} is the inverse of the covariance matrix S formed by vectors I and J.

$$HDI_i = e^{-(D_{ij})^{-1}} \tag{9}$$

HDI_i represents the HDI of key characteristic variables. A larger distance $D_{ij} = diatance\,(I|J)$ indicates a higher degree of health degradation in the unit; conversely, a smaller distance indicates a lower degree of health degradation in the unit.

Multi-source HDI fusion based on multi-objective optimization

The operational condition of the unit changes in real time, and the impact of each monitoring parameter on the unit's health status also varies over time. Traditional comprehensive evaluation methods typically treat each indicator with equal weight or use an entropy-based weighting method [39]. However, due to the unique inherent and dynamic characteristics of different indicators, simple weighted fusion does not fully reflect the actual impact of each indicator on the evaluation results. To address this issue, this study employs the NSGA-II algorithm to solve for the optimal weight vector and constructs the RCHDI by weighted fusion of multi-source HDIs. This allows for a more comprehensive and real-time representation of the health status changes in PSUs.

Objective functions and constraints

Information entropy is a measure of the randomness or uncertainty of a system, used to ensure the diversity and balance of weight distribution, such that no single indicator excessively dominates the RCHDI. For the weighted HDI data, information entropy $f_1(x)$ is defined as:

$$f_1(x) = -\sum_{i=1}^{n} P_i log\,(p_i) \tag{10}$$

Where, P_i represents the proportion of the i-th feature's weight relative to the sum of all weights, calculated as $P_i = \frac{x_i}{\sum_{j=1}^{n} x_j}$. In this equation, x_i is the weight of the i-th feature, and n is the total number of features.

Measuring the variance of weighted health indicators can assess the variability of the health index over time. Higher variance indicates that the health status may be unstable; appropriate weight configurations can reduce fluctuations and enhance the stability of health assessments. Variance $f_2(x)$ is defined as:

$$f_2(x) = var\left(\sum_{i=1}^{n} x_i \cdot HDI_i\right) \tag{11}$$

Where, var represents the calculation of variance.

Negative covariance is the negative value of the covariance between two variables. Covariance is a statistical measure used to assess the direction and extent of the joint variation between two variables. By minimizing negative covariance in optimization, the positive correlation between the comprehensive health index and key health indicators can be enhanced, thereby improving the accuracy and robustness of health assessments. Negative covariance $f_3(x)$ is defined as:

Let the comprehensive health index $f$be calculated from the weighted health indicators:

$$f = \sum_{i=1}^{n} x_i \cdot HDI_i \tag{12}$$

The objective function for negative covariance $f_3(x)$ calculates the negative sum of the covariances between the comprehensive health index and all key health indicators, as follows:

$$f_3(x) = -\sum_{i=1}^{n} Cov\,(f, HDI_i) \tag{13}$$

where the covariance is calculated as:

$$Cov\,(f, HDI_i) = \frac{1}{T-1}\sum_{t=1}^{T}\left(f_t - \bar{f}\right)\left(HDI_{it} - \bar{HDI}_i\right) \tag{14}$$

where: T is the number of time points; f_t is the value of the comprehensive health index at time point t; $\bar{f}$ is the mean of the comprehensive health index; $\bar{HDI}_i$ is the mean of the i-th key health indicator.

Combining entropy, variance, and negative covariance according to equations (10)、(11)、(13), a multi-objective function can be constructed to determine weights for critical health indicators, with the following constraints added:

$$\begin{cases} min\left[f_1(x)\ , f_2(x)\ , f_3(x)\right] \\ \sum_{i=1}^{n} x_i = 1 \\ x_i \geq\ 0, i = 1,2,\ldots\ , n \end{cases} \tag{15}$$

Where, $f_1(x)$ represents entropy, $f_2(x)$ denotes the variance function, $f_3(x)$ stands for the negative covariance function.

Finally, Optimize the multi-objective function in Eq. (15) using the NSGA-II algorithm from Sect. 2.3 to find the optimal weight vector for evaluating indices.

Engineering application and analysis

Data description

The pump station discussed in this study is a key water transfer site within the Middle Route of the South-to-North Water Diversion Project. The total design flow rate of the pump station is 20.00 m^3/s, with each unit designed for 6.67 m^3/s. It employs four units of vertical axial flow pumps of model 1600ZLQ6.67-1.60, one of which is standby. The design head is 2.21 m, with each pump unit paired with a motor rated at 355 kW. The total installed capacity of the pump station is 1420 kW. The station is powered by a dual-loop 10 kV electrical supply.

Since it's operation, the Pump Station has accumulated a large amount of available historical time series data. This data is generated and collected by the industrial control system, stored in the form of time series data for industrial control points, with frequencies ranging from $100\,ms$ to 1000 ms. For a view of some components and sensor arrays, please refer to Fig. 6.

The main units monitored at the pump station include the pumps and motors. The types of monitoring data for the unit are listed in Table 1 and include: motor vibration、 pump vibration、coupling noise、pump noise、stator winding temperature、thrust bearing temperature、upper and lower guide bearing temperatures、stuffing box temperature、lower oil sump oil temperature、upper oil sump oil temperature、lower oil sump oil level、upper oil sump oil level、current、voltage、active power and unit vibration amplitude, totaling 42 dimensions.

Data preprocessing

During the period from Jan 20, 2023, to Oct 11, 2023, the industrial control system of the pump station collected 204,559 real measurement values. However, the actual measured data significantly differed from experimental simulation data, showing noticeable data anomalies and rapid shifts. According to the 3 Sigma principle of the normal distribution, data points exceeding three times the standard deviation from the mean were defined as outliers and replaced with three times the standard deviation. Additionally, the data was down sampled to 1 sample per minute and filtered to remove invalid data due to sensor malfunctions and other reasons. As a result, the final dataset consisted of 101,186 valid annotated data points.

To enhance the accuracy and timeliness of health assessment for the pump station units, it is essential to leverage spatiotemporal complementarity among parameters and simplify redundant ones when constructing the health assessment model. In health assessment, operational states are commonly described using active power information. Therefore, key monitoring parameters most correlated with active power are selected as health assessment indicators. The random forest algorithm[40] is employed to assess feature importance and conduct feature selection. The Gini index measures the contribution of a feature in reducing the impurity of the model, effectively identifying the key features that have the most impact on decision-making. The Gini index (importance contribution) of each data feature is shown in Table 2.

From Table 2, it can be observed that there is a significant variation in the Gini index contributions of each monitoring parameter. The Gini index contribution of thrust bearing temperature is highest, approximately 0.5321, while the stator winding temperature has the lowest contribution, around 0.0025, indicating minimal impact on the operational power of the PSUs. To better reflect the actual health condition of the units, based on the feature importance ranking, the final selection of 6 monitoring features with contribution values greater than 0.02 are chosen as key health assessment indicators: Thrust Bearing Temperature, Motor X-axis Vibration, Lower Guide Bearing Temperature, Technical Water Pump Temperature, Pump X-axis Oscillation, and Upper Guide Cooling Water Temperature.

Health baseline model (HBM) evaluation

To validate the superior performance of the proposed graph-based Health Baseline Model (HBM), a comparative experiment was designed. The comparison models include Autoformer [41], Informer[42], Dlinear[43], and MSGNet [44]. The initial learning rate was set to 0.001, and the training period was set to 300 epochs. The training data was split into 70% for training and 30% for testing. The data was normalized in batches before being loaded into the models for training. Performance evaluation was conducted using three metrics: Mean Absolute Error (MAE), Root Mean Square Error (RMSE), and Mean Squared Error (MSE).

From Table 3, compared to the MSGNet model, the CrossGNN model showed reductions of 0.04, 0.41, and 1.45 in the MAE, RMSE, and MSE metrics respectively, achieving the best results in both MAE and RMSE. This indicates that the model has the lowest average error and highest stability. Compared to Transformer models based on attention mechanisms, graph representation learning better captures the internal relationships within high-dimensional time series parameters, effectively enhancing the capability to represent states and significantly improving task accuracy. Experimental results confirm the superior performance of the CrossGNN model in health monitoring of pump station units.

To reduce the impact of random initialization on accuracy, we conducted ten runs of the same model to obtain the mean and standard deviation of performance metrics, as shown in Fig. 7. Multiple tests demonstrate that CrossGNN not only offers the highest prediction accuracy but also exhibits higher stability. In the ranking of

Fig. 6. Schematic diagram of PSUs components and sensor array on site.

prediction accuracy on the PSUs dataset, CrossGNN performs the best, followed by MSGNet, Dlinear, Informer, and Autoformer. Overall, Autoformer and Informer models, which are based on attention mechanisms, tend to over-rely on contextual information and are susceptible to noise interference, making it difficult to accurately capture the intrinsic information of coupled variables, resulting in significant prediction errors. In contrast, models based on graph neural networks show minor losses but greater variability in accuracy. CrossGNN with its shortest boxplot length and lowest bottom, demonstrates optimal precision and stability. This is attributed to its ability to learn dependencies across different scales and invariant relationships between homogeneity and heterogeneity among variables, which enhances the model's robustness to noise.

Construction of real-time comprehensive health degradation index

Construction of health degradation index

With the completion of the HBM, the real-time operational status's 42-dimensional monitoring parameters are input into the model, and the key monitoring parameters {Thrust Bearing Temperature, Motor X-axis Vibration, Lower Guide Bearing Temperature, Technical Water Pump Temperature, Pump X-axis Oscillation, Upper Guide Cooling Water Temperature} are used as output labels, representing theoretical health prediction values.

The assessment sample set consists of valid data collected from Jun 1, 2023, to Oct 1, 2023. Data was gathered every minute, with each data point representing one minute. Every 60 data points were used to generate one GCM as a set of assessment samples, totaling 2500 assessment units. For each key measurement point, the HDI is calculated separately: Thrust Bearing Temperature HDI (HDI_tbt)、Motor X-axis Vibration HDI (HDI_mxv)

Symbol	Monitored parameters	Symbol	Monitored parameters
ugbt	Upper guide bearing temperature	pv	Pump vibration
ugott	Upper guide oil tray temperature	mvx	Motor X-axis vibration
ugcwt	Upper guide cooling water temperature	mlo	Motor lower oil level
V	Voltage	mn	Motor noise
I	Current	muo	Motor upper oil level
tbt	Thrust bearing temperature	myv	Motor Y-axis vibration
cpf	Cumulative pump flow	lgott	Lower guide oil tray temperature
swt	Stator winding temperature	pecr	Pump energy consumption ratio
rcf	Reverse cumulative flow	pep	Pump electric power
isf	Instantaneous second flow	cln	Coupling layer noise
bmt	Blade mechanism temperature	ps	Pump swing
p	Pump active power	pcwp	Pump cooling water pressure
mott	Maximum oil tray temperature	ppf	Pump power factor
prp	Pump reactive power	pbt	Packing box temperature
fcwt	Frequency converter winding Temperature	lgcwt	Lower guide cooling water temperature
ps	Pump speed	lgbt	Lower guide bearing temperature
fcc	Frequency converter current	cwf	Cooling water flow
fcp	Frequency converter power	cwmpp	Cooling water main pipe pressure
fcat	Frequency converter ambient Temperature	tsput	Technical supply pump unit temperature
fcv	Frequency converter voltage	swmpt	Supply water main pipe temperature
asp	Air System Pressure	vpp	Vacuum pipeline pressure

Table 1. Types of monitoring data for unit.

Function	Importance	Function	Importance
Thrust bearing temperature	0.5321	Lower guide cooling water temperature	0.0153
Motor X-axis vibration	0.1317	Pump Y-axis swing	0.0099
Lower guide bearing temperature	0.1164	Motor Y-axis vibration	0.0075
Technical supply pump temperature	0.1012	Blade mechanism temperature	0.0039
Pump X-axis swing	0.0465	Pump oil tray temperature	0.0028
Upper guide cooling Water temperature	0.0226	Motor lower oil level	0.0025

Table 2. The gini index contributions of each data feature.

Model	MAE	RMSE	MSE
Informer	1.6293	9.7417	94.9014
Autoformer	0.4781	10.8632	118.0096
MSGNet	0.1571	1.9696	3.8792
Dlinear	0.2342	2.1498	4.6215
CrossGNN	0.1152	1.5592	2.4310

Table 3. Comparison of health benchmark model experimental results.

、Lower Guide Bearing Temperature HDI (HDI_lgbt)、Technical Supply Pump Temperature HDI (HDI_tsput)、Pump X-axis Swing HDI (HDI_pxs)、Upper Guide Cooling Water Temperature HDI (HDI_ugcwt).

Figure 8 illustrates the Health Index (HDI) trends for 6 key monitoring parameters of the pump station unit. While local fluctuations are present, there is an overall upward trend, indicating changes in the unit's health status over time. The HDI for HDI_mxv and HDI_lgbt shows a gradual increase, with HDI_mxv rising from approximately 0.20 to 0.56, and HDI_lgbt increasing from about 0.10 to 0.52. This suggests sustained stability with minor performance degradation, necessitating regular inspections to prevent structural defects or increased wear. In contrast, parameters such as HDI_tbt、HDI_tsput, HDI_pxs and HDI_ugcwt exhibit more significant fluctuations. Notably, the HDI_pxs fluctuates widely between 0.20 and 0.47, indicating potential issues like improper assembly or mechanical wear. These fluctuations highlight the need for stricter monitoring and maintenance strategies.

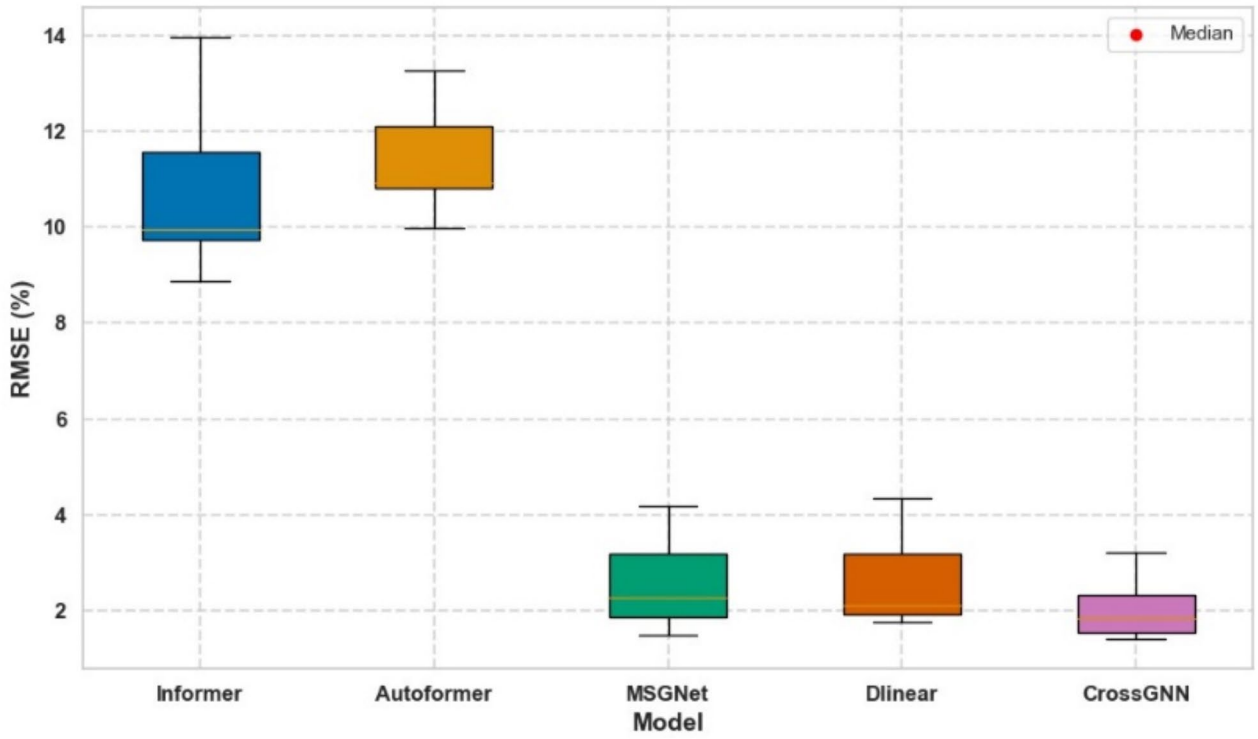

Fig. 7. Comparison of health benchmark prediction model performance.

Overall, continuous monitoring and analysis of these parameters are essential to promptly identify and address potential mechanical failures, minimizing unscheduled downtime and ensuring operational efficiency and safety.

Construction of RCHDI

Figure 8 shows that the HDI curves for different monitoring indicators vary, indicating that a single indicator or average weight cannot provide an accurate and comprehensive response to the overall changes in the unit. Therefore, it is necessary to extract different degradation representation information from various signals and perform weighted fusion. As described in Sect. 3.3, a multi-objective weight-solving function is constructed according to Eqs. (10), (11), (12), (13), (14) and (15), and solved using the NSGA-II algorithm. The specific operations are as follows: the population size is set to 100, with a maximum of 10,000 iterations, and 50 exponential weight vector individuals are formed as the initial population through random mutation. Individual selection is based on the fitness function, and genetic operations are carried out using binary crossover and polynomial mutation operators, with a crossover rate of 0.9 and a mutation rate of 0.01, meaning that 1% of genes undergo mutation each generation. An elitism strategy is employed, where superior individuals are selected through fast non-dominated sorting and crowding distance comparison, ensuring these individuals evolve into the next generation. After 40 iterations, the algorithm achieves a Pareto optimal solution set, with the optimization results displayed in Fig. 9.

As shown in Fig. 9, $f_1(x)$ represents entropy, $f_2(x)$ denotes the variance function, $f_3(x)$ stands for the negative covariance function. The non-dominated solutions are highlighted in red, and the best weight vector is obtained based on the predefined importance levels, as shown in Table 4.

Figure 10 shows the RCHDI curve calculated using the optimal weights, integrating the characteristics of 6 key monitoring parameters. It exhibits local fluctuations and a gradually increasing overall trend, consistent with the actual health status. This demonstrates that the method proposed in this paper is practical and can accurately reflect the actual operating conditions of the unit.

This study uses 6 key monitoring parameters to calculate the RCHDI for a quantitative analysis of the health status of PSUs. As shown in Fig. 10, since the start of the operational period, RCHDI has continuously deteriorated, gradually increasing from 0.1 at the beginning of the evaluation period to 0.4. This change indicates that the degradation of thrust bearings, technical supply pumps, pump rotors, and upper guide bearings has led to a decline in the overall health of the unit. Particularly after a period of relative stability in the data between 1000 and 1500 days, the sharp rise in the RCHDI index highlights the necessity for urgent maintenance. The comparison between the original weighted data and the smoothed data further confirms the long-term degradation trend of the equipment's health and effectively reduces the impact of short-term fluctuations on the health assessment. Although the HDI increases with operational time, typically, degradation indicators can be restored through maintenance and servicing once a certain level of degradation is reached. It is important to note

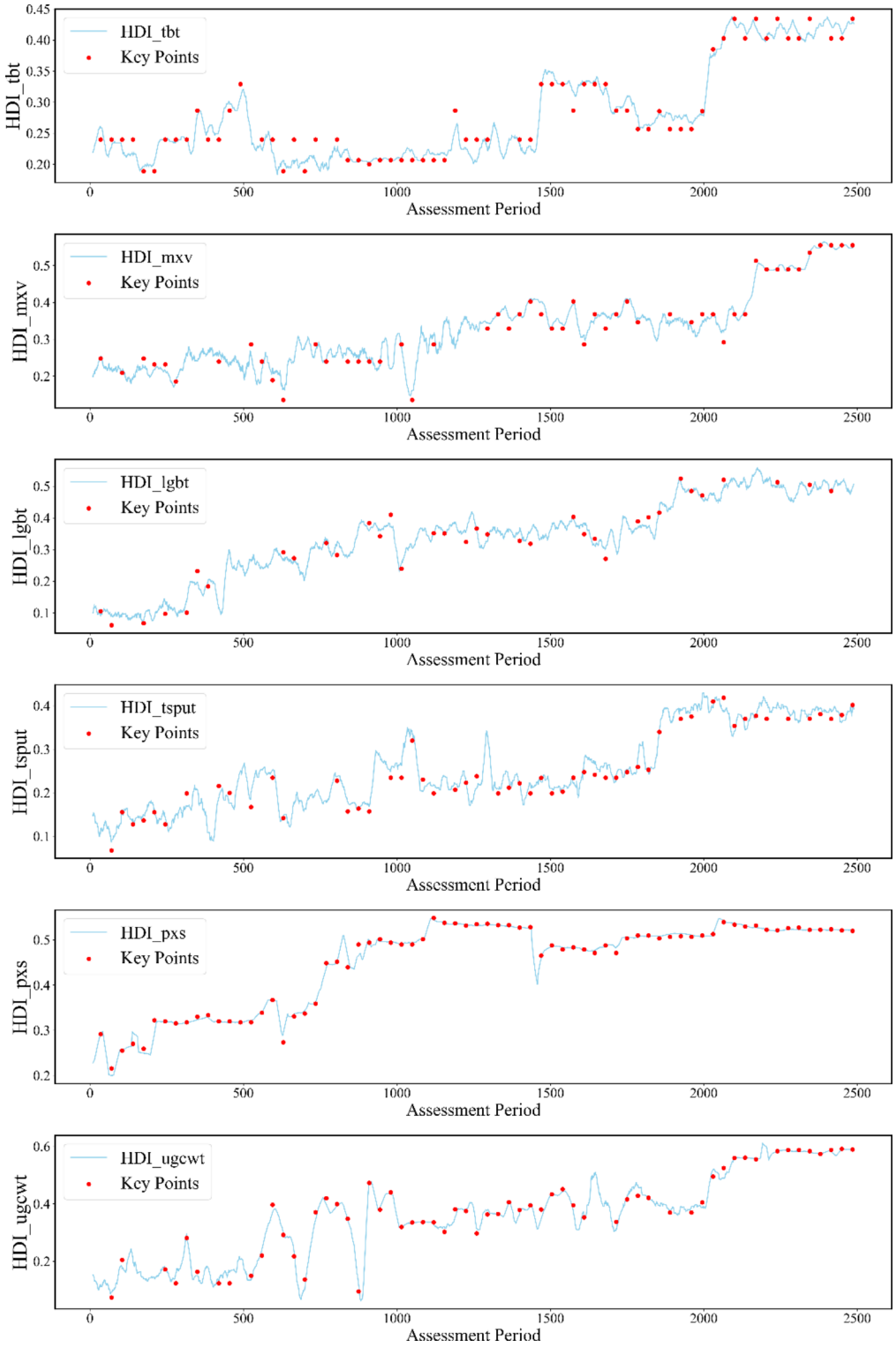

Fig. 8. Trends in HDI for different monitoring parameters.

that the data collected in this study did not include maintenance periods, so no regression phenomenon in HDI indices was observed, effectively characterizing the unit's degradation state.

The continuous trend of health degradation may be caused by wear and tear of internal components, insufficient maintenance, or operational errors. This study determines the timing for maintenance interventions through periodic evaluations and preset thresholds. When RCHDI exceeds the set threshold, maintenance should be triggered immediately. Adjusting the maintenance cycle based on real-time data effectively addresses potential faults, optimizing operational efficiency and extending the equipment's lifespan.

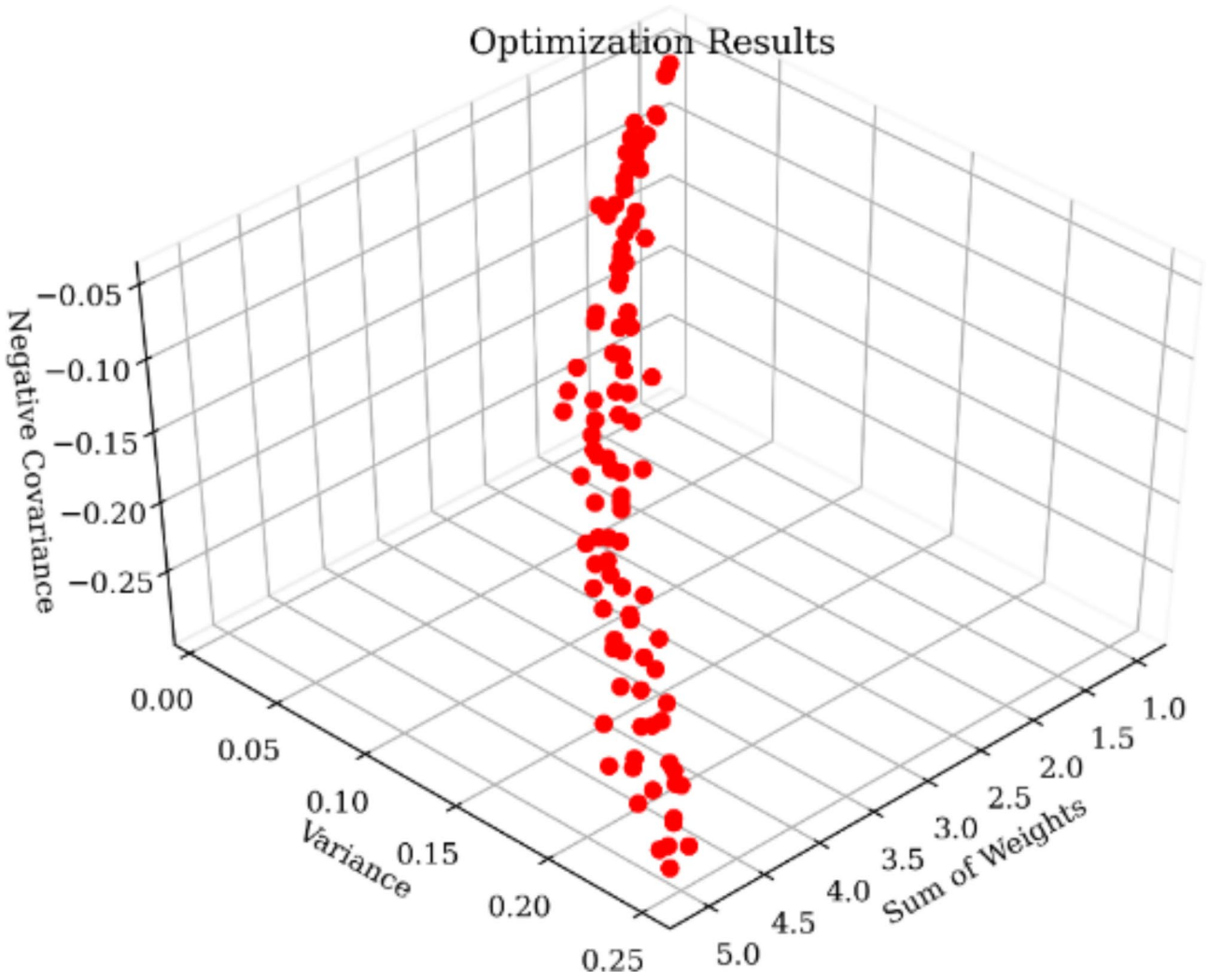

Fig. 9. Optimized solution set of NSGA-II algorithm.

Variable	a	b	c	d	e	f
Weight	0.2128	0.1812	0.0893	0.4038	0.0156	0.1135

Table 4. Weights of key monitoring indicators.

Discussion

Comparison of different distance calculation methods

The effectiveness of the proposed RCHDI construction technique based on MD-GCM was tested by comparing it with the RCHDI construction method based on Relative Standard Deviation (RSD)[45]. The RCHDI based on relative deviation is defined as follows:

$$RSD = \frac{|y_i - \widehat{y}_i|}{\widehat{y}_i} \times 100\% \tag{16}$$

In the formula, y_i represents the actual measured value of the key monitoring parameter at the current time, and $\widehat{y}_i$ represents the theoretical healthy value predicted by the health benchmark model.

To quantify the impact of deviations calculated using RSD and MD-GCM on the RCHDI curve, STA (Stability) and SMO (Smoothness) are used as the criteria for curve stability and smoothness, defined as follows[46]:

$$STA = \sqrt{\frac{1}{n}\sum_{i=1}^{n}\left(I_i - \bar{I}\right)^2} \tag{17}$$

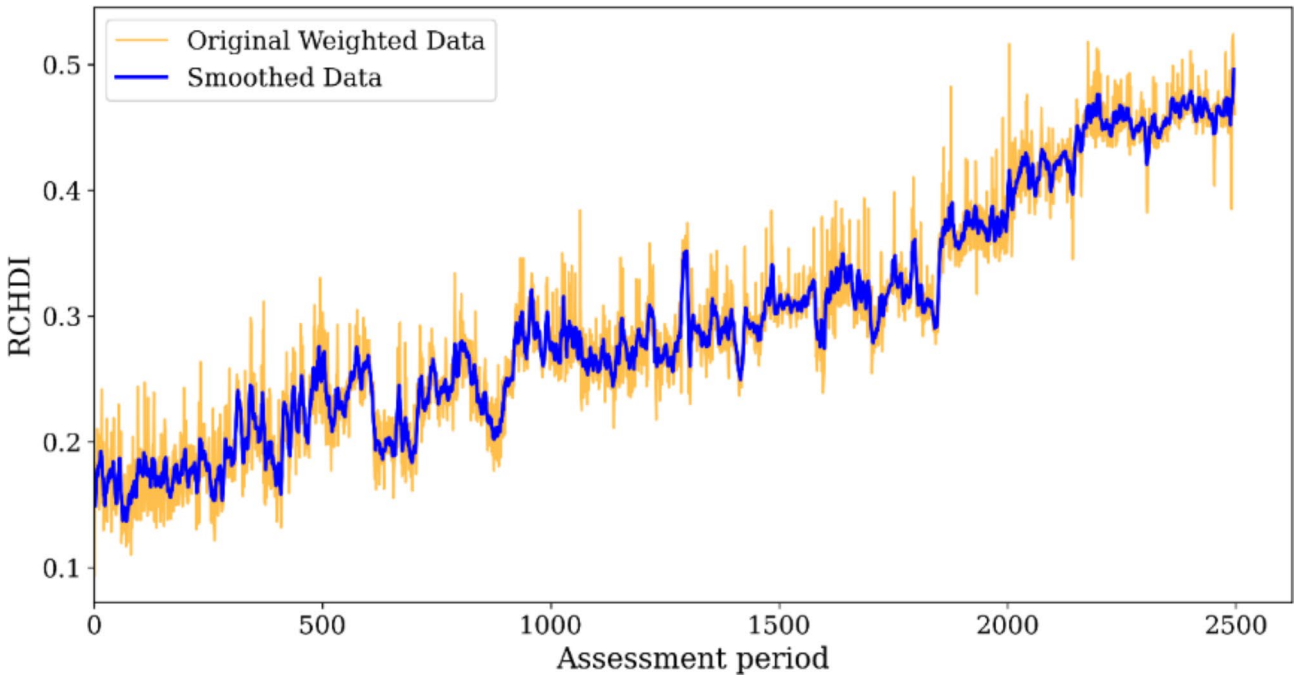

Fig. 10. Real-time comprehensive degradation curve.

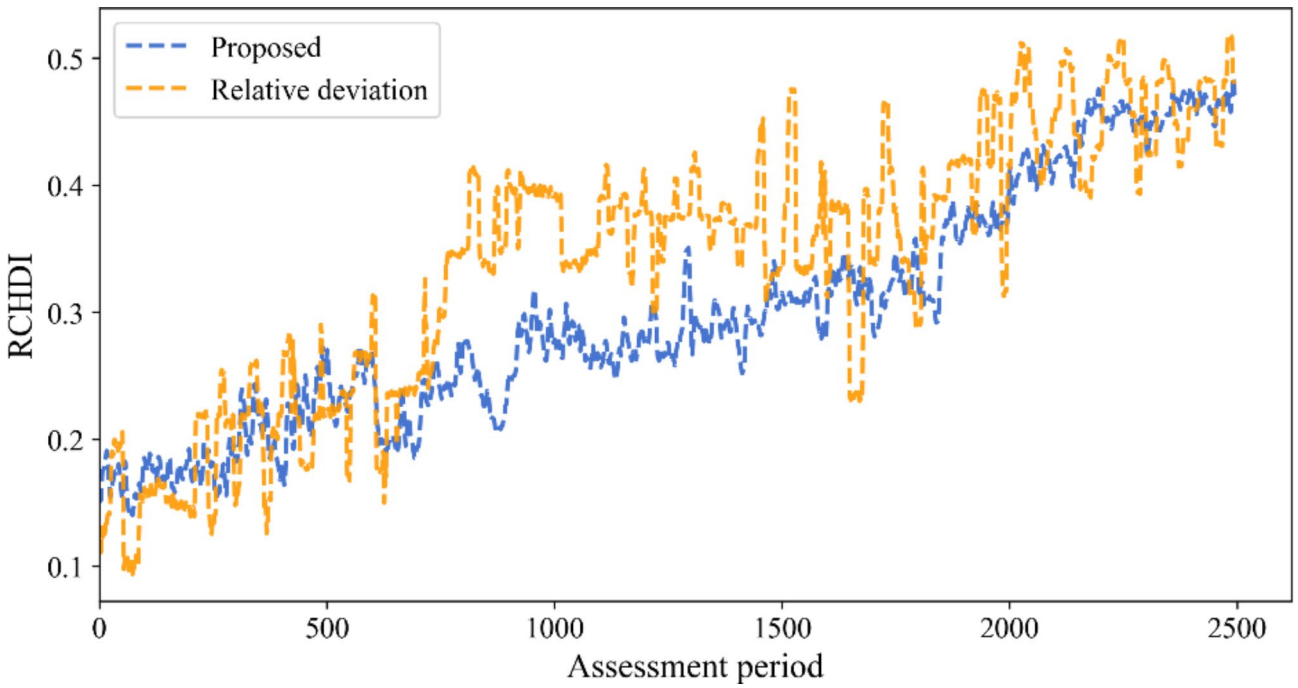

Fig. 11. Comparison of different HDI methods.

$$SMO = \frac{\sum_{i=1}^{n-1} |I_{i+1} - I_i|}{n-1} \tag{18}$$

In the formula, I_i and $\bar{I}$ represent the value of each point on the curve and its average value, respectively, and n represents the number of samples.

Figure 11 depicts the estimated RCHDI curve, while Table 5 illustrates the evaluated STA and STO values. The RCHDI curve based on relative deviation exhibits significant fluctuations, whereas the RCHDI curve of

Methods	STA	STO
MD-GCM	0.0903	0.0037
RSD	0.1146	0.0070

Table 5. Stability and smoothness of different HDI methods.

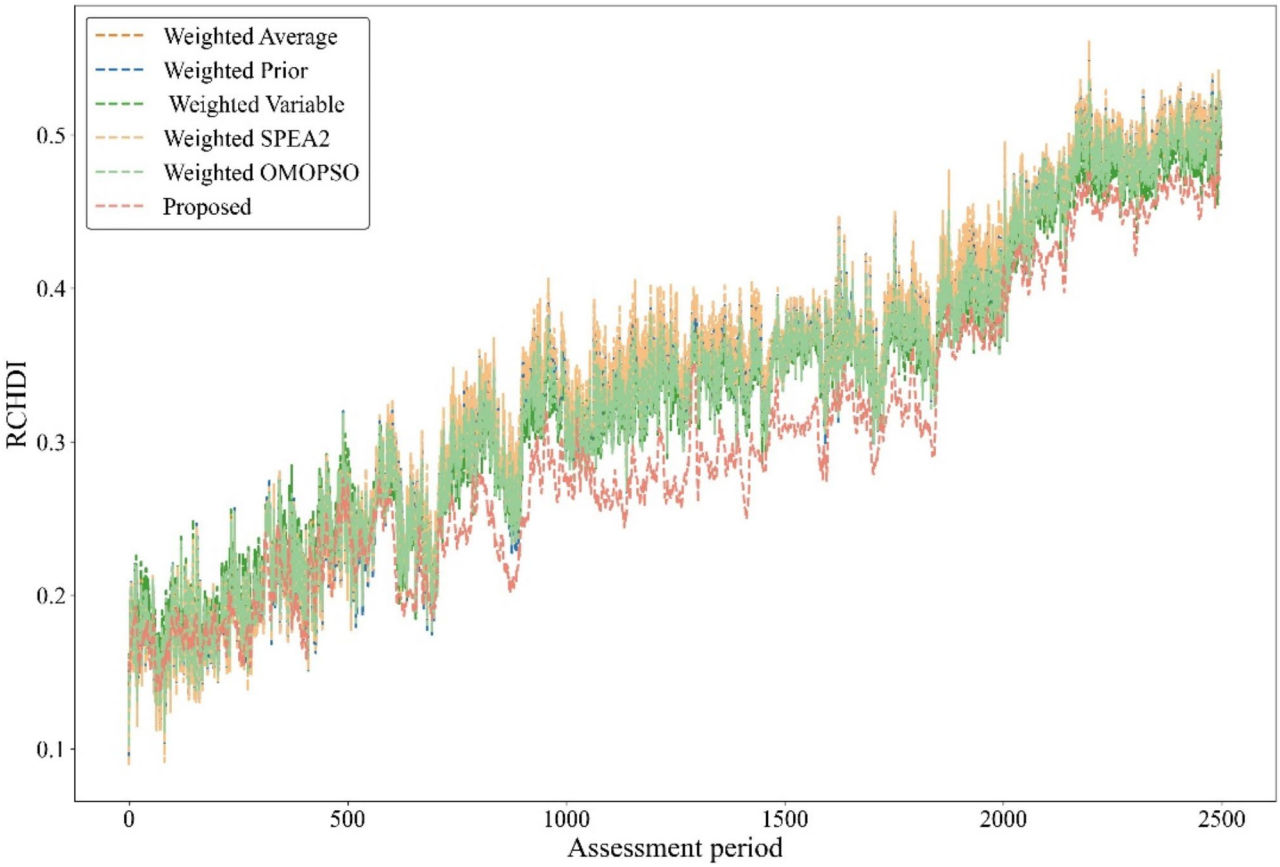

Fig. 12. Comparison of different weighting methods.

the proposed method is smoother and more accurately reflects the deterioration process of health conditions. Furthermore, the STA and STO of the proposed method are significantly lower than those based on relative deviation, with the stability and smoothness of the curve improved by 21.5% and 47.1%, respectively. This is because the proposed method quantifies the uncertainty information contained in the amplitude magnitude and reflects changes in the amplitude of state monitoring parameters, both quantitatively and qualitatively describing the randomness of signal changes, thereby better characterizing the variations in the unit's health performance.

The smoother RCHDI curve obtained through the proposed method indicates a more reliable and accurate assessment of the health degradation process. Enhanced curve smoothness and stability are crucial for early fault detection and timely maintenance. This method reduces relative deviation and provides a clearer trend, aiding in the development of more effective maintenance plans, thereby extending the operational efficiency and lifespan of PSUs. Additionally, the method's quantitative and qualitative analysis of signal randomness offers a comprehensive understanding of health status changes, ensuring full consideration of minor fluctuations and major trends, highlighting its superiority in monitoring and maintaining the health of complex mechanical systems.

Comparison of different RCHDI weight calculation methods

The proposed multi-objective optimization weight calculation method was tested against traditional methods such as weighted average, weighted prior, and weighted variable, as well as multi-objective optimization algorithms SPEA2 and OMOPSO.

Based on the results shown in Fig. 12; Table 6, different weighting methods demonstrated consistency in the overall trend, all indicating a gradual increase in RCHDI over the assessment period, reflecting the continuous degradation of equipment health. In the comparative analysis, NSGA-II demonstrated significant advantages. Particularly in comparison with SPEA2 and OMOPSO, NSGA-II displayed superior stability and smoothness.

Weights method	STA	SMO
Average	0.0963	0.0178
Prior	0.1014	0.0201
Variable	0.0930	0.0163
SPEA2	0.1101	0.0242
OMOPSO	0.0978	0.0186
Proposed	0.0903	0.0137

Table 6. Results of different weighting methods.

Specifically, SPEA2 had a stability (STA) of 0.1101 and smoothness (SMO) of 0.0242, while OMOPSO had a stability of 0.0978 and smoothness of 0.0186, both higher than NSGA-II (STA = 0.0903, SMO = 0.0137). This indicates that the proposed method reduces the impact of short-term fluctuations and more smoothly reflects the long-term degradation trend of the equipment. By integrating the inherent attributes and real-time dynamic characteristics of each indicator, the proposed method dynamically adjusts weights, better adapting to various changes during actual operations, thereby enhancing the reliability and accuracy of the assessment.

In contrast, weighted average, weighted prior, and weighted variable methods use fixed weight configurations and show limitations in dynamic equipment states, as they cannot adapt to changes in environmental or equipment conditions, potentially leading to inaccurate assessments. The external archive strategy of SPEA2 and the particle swarm optimization characteristics of OMOPSO lack adaptability in dynamically adjusting weights to accommodate real-time data, particularly in fine exploration and multi-objective trade-offs. Although capable of capturing the overall trend, they exhibit greater volatility, which could lead to misjudgments or over-maintenance. Meanwhile, NSGA-II, through its non-dominated sorting and crowding distance mechanisms, maintains high efficiency in global searches while quickly converging to the Pareto optimal front, effectively balancing the exploration and exploitation of solutions. This advantage enables NSGA-II to more accurately reflect the actual health status of equipment in complex multi-objective optimization tasks, particularly when dealing with indicators closely related to equipment health.

Conclusion

This paper proposes an innovative method for real-time comprehensive evaluation of PSUs health status based on spatiotemporal fusion and uncertainty information, encompassing four steps: HBM construction, key monitoring parameter selection, multi-source HI construction, and real-time comprehensive evaluation. The results indicate:

(1) Utilizing CrossGNN to construct the HBM not only mitigates sensor data distortion and operational noise issues but also captures dynamic correlations and heterogeneity of multi-dimensional variable sequences more accurately through cross-scale and cross-variable interactions.

(2) Key monitoring parameters closely related to the operational state are selected using the random forest method to build a health HSA index system, providing a more realistic and comprehensive response to the unit's health status. The proposed dynamic multi-objective optimization weighting method integrates the intrinsic and dynamic characteristics of each indicator, achieving the lowest STA (0.0903) and SMO (0.0037) values.

(3) The method qualitatively and quantitatively describes the changes in monitoring parameters and their uncertainty information. The new RCHDI based on MD-GCM comprehensively reflects changes in the actual operational state, improving curve stability and smoothness by 21.5 and 47.1%, respectively. In summary, the proposed method offers significant engineering application value, enabling real-time understanding of health status changes and providing technical support for condition prediction and maintenance planning.

However, a major issue in applying HSA tasks on-site is poor data quality. High anomalies and miss rates in field data result in limited standardized data. Future research should focus on leveraging high-fidelity data enhancement methods to obtain high-quality pseudo-data from field data.

Data availability

Data are fully available through the corresponding author upon reasonable request.

Received: 25 July 2024; Accepted: 27 September 2024
Published online: 15 October 2024

References

1. Tse, H. Challenges for pumping station design in water industries: an overview of impacts from climate change and energy crisis. *Water Res.* **253**, 121250. https://doi.org/10.1016/j.watres.2024.121250 (2024).
2. Kong, L. et al. Predictive control for the operation of cascade pumping stations in water supply canal systems considering energy consumption and costs. *Appl. Energy*. **341**, 121103. https://doi.org/10.1016/j.apenergy.2023.121103 (2023).
3. Zhang, F., Liu, J., Liu, Y., Li, H. & Jiang, X. Data-model-interactive enhancement-based Francis turbine unit health condition assessment using graph driven health benchmark model. *Expert Syst. Appl.* **249**, 123724. https://doi.org/10.1016/j.eswa.2024.123724 (2024).
4. Zhang, X., Jiang, Y., Wang, X. B., Li, C. & Zhang, J. Health condition assessment for pumped storage units using multihead self-attentive mechanism and Improved radar chart. *IEEE Trans. Industr. Inf.* **18**, 8087–8097. https://doi.org/10.1109/TII.2022.3165642 (2022).

5. Cordova, M. M., Finardi, E. C., Ribas, F. A. C., de Matos, V. L. & Scuzziato, M. R. Performance evaluation and energy production optimization in the real-time operation of hydropower plants. *Electr. Power Syst. Res.* **116** https://doi.org/10.1016/j.epsr.2014.06.012 (2014).
6. Huang, H. et al. The prediction method on the early failure of hydropower units based on gaussian process regression driven by monitoring data. *Appl. Sci.* **11** (1), 153. https://doi.org/10.3390/app11010153 (2021).
7. Shan, Y., Liu, J., Xu, Y. & Zhou, J. A combined multi-objective optimization model for degradation trend prediction of pumped storage unit. *Measurement* **169**, 108373. https://doi.org/10.1016/j.measurement.2020.108373 (2021).
8. An, X., Yang, L. & Pan, L. Nonlinear prediction of condition parameter degradation trend for hydropower unit based on radial basis function interpolation and wavelet transform, Proceedings of the Institution of Mechanical Engineers, Part C: Journal of Mechanical Engineering Science, 229 3515–3525. (2015). https://doi.org/10.1177/0954406215570771
9. Cerrada, M. et al. A review on data-driven fault severity assessment in rolling bearings. *Mech. Syst. Signal Process.* **99**, 169–196. https://doi.org/10.1016/j.ymssp.2017.06.012 (2018).
10. Wei, Y., Wu, D. & Terpenny, J. Learning the health index of complex systems using dynamic conditional variational autoencoders. *Reliab. Eng. Syst. Saf.* **216**, 108004. https://doi.org/10.1016/j.ress.2021.108004 (2021).
11. Manjurul Islam, M. M., Prosvirin, A. E. & Kim, J. M. Data-driven prognostic scheme for rolling-element bearings using a new health index and variants of least-square support vector machines. *Mech. Syst. Signal Process.* **160**, 107853. https://doi.org/10.1016/j.ymssp.2021.107853 (2021).
12. Yang, F., Habibullah, M. S. & Shen, Y. Remaining useful life prediction of induction motors using nonlinear degradation of health index. *Mech. Syst. Signal Process.* **148**, 107183. https://doi.org/10.1016/j.ymssp.2020.107183 (2021).
13. Yan, T. et al. Fisher's discriminant ratio based health indicator for locating informative frequency bands for machine performance degradation assessment. *Mech. Syst. Signal Process.* **162**, 108053. https://doi.org/10.1016/j.ymssp.2021.108053 (2022).
14. Zhang, X., Jiang, Y., Li, C. & Zhang, J. Health status assessment and prediction for pumped storage units using a novel health degradation index. *Mech. Syst. Signal Process.* **171**, 108910. https://doi.org/10.1016/j.ymssp.2022.108910 (2022).
15. An, X., Pan, L. & Yang, L. Condition parameter degradation assessment and prediction for hydropower units using Shepard surface and ITD. *Trans. Inst. Meas. Control* **36**, 1074–1082. https://doi.org/10.1177/0142331214532998 (2014).
16. Fu, W. et al. A state tendency measurement for a hydro-turbine generating unit based on aggregated EEMD and SVR. *Meas. Sci. Technol.* **26**, 125008. https://doi.org/10.1088/0957-0233/26/12/125008 (2015).
17. Yan, S. et al. A new machinery anomaly detection method towards complex operating conditions. *Reliab. Eng. Syst. Saf.* **236**, 109319. https://doi.org/10.1016/j.ress.2023.109319 (2023).
18. Ye, Z. & Yu, J. Health condition monitoring of machines based on long short-term memory convolutional autoencoder. *Appl. Soft Comput.* **107**, 107379. https://doi.org/10.1016/j.asoc.2021.107379 (2021).
19. Duan, R., Liu, J., Zhou, J., Wang, P. & Liu, W. An Ensemble Prognostic Method of Francis Turbine units using low-Quality Data under Variable operating conditions. *Sensors*. **22** (2), 525. https://doi.org/10.3390/s22020525 (2022).
20. Hamilton, W. L., Ying, R. & Leskovec, J. Inductive representation learning on large graphs. *Adv. Neural. Inf. Process. Syst.*, pp. 1025–1035. (2017).
21. LeClair, A., Haque, S., Wu, L. & McMillan, C. Improved Code Summarization via a Graph Neural Network, Proceedings of the 28th International Conference on Program Comprehension, Association for Computing Machinery, Seoul, Republic of Korea, pp. 184–195. (2020). https://doi.org/10.1145/3387904.3389268
22. He, X. et al. LightGCN: Simplifying and Powering Graph Convolution Network for Recommendation, SIGIR 2020 - Proceedings of the 43rd International ACM SIGIR Conference on Research and Development in Information Retrieval, pp. 639–648. (2020). https://doi.org/10.1145/3397271.3401063
23. Zhang, J., Meng, H., Gu, B. & Li, P. Research on short-term wind power combined forecasting and its gaussian cloud uncertainty to support the integration of renewables and EVs. *Renew. Energy*. **153**, 884–899. https://doi.org/10.1016/j.renene.2020.01.062 (2020).
24. Chu, Z. et al. An operation health status monitoring algorithm of special transformers based on BIRCH and Gaussian Cloud methods. *Energy Rep.* **7**, 253–260. https://doi.org/10.1016/j.egyr.2021.01.072 (2021).
25. Xu, X. et al. A cloud model-based interval-valued evidence fusion method and its application in fault diagnosis. *Inf. Sci.* **658**, 119995. https://doi.org/10.1016/j.ins.2023.119995 (2024).
26. Dai, J. et al. An optimized method for variational autoencoders based on Gaussian cloud model, Information Sciences, 645 119358. https://doi.org/10.1016/j.ins.2023.119358, A two-stage solution method based on NSGA-II for Green Multi-Objective integrated process planning and scheduling in a battery packaging machinery workshop, Swarm and Evolutionary Computation, 61 (2021) 100820. https://doi.org/10.1016/j.swevo.2020.100820 (2023).
27. X. Wen, K. Wang, H. Li, H. Sun, H. Wang, L. Jin, A two-stage solution method based on NSGA-II for Green Multi-Objective integrated process planning and scheduling in a battery packaging machinery workshop, Swarm and Evolutionary Computation, 61 (2021) 100820
28. Jiwapatria, S. et al. Multi-objective optimization of active control system using population guidance and modified reference-point-based NSGA-II. *Results Control Optim.* **16**, 100453. https://doi.org/10.1016/j.rico.2024.100453 (2024).
29. Tang, X. et al. Multi-objective optimization model of Ultra-high voltage direct current system considering low carbon and equipment safety based on Im-NSGA-II and ResNet-LSTM. *Comput. Electr. Eng.* ,118(2024)https://doi.org/10.1016/j.compeleceng.2024.109441
30. Ye, L. et al. A multi-objective optimization approach for battery thermal management system based on the combination of BP neural network prediction and NSGA-II algorithm. *J. Energy Storage* **99**, 113212. https://doi.org/10.1016/j.est.2024.113212 (2024).
31. Yazdinejad, A., Dehghantanha, A., Parizi, R. M. & Epiphaniou, G. An optimized fuzzy deep learning model for data classification based on NSGA-II, Neurocomputing, 522 116–128 (2023). https://doi.org/10.1016/j.neucom.2022.12.027
32. Wang, Y. J., Wang, G. G., Tian, F. M., Gong, D. W. & Pedrycz, W. Solving energy-efficient fuzzy hybrid flow-shop scheduling problem at a variable machine speed using an extended NSGA-II. *Eng. Appl. Artif. Intell.* **121**, 105977. https://doi.org/10.1016/j.engappai.2023.105977 (2023).
33. Leng, Y. J., Li, X. S. & Zhang, H. A novel evaluation method for renewable energy plans. *Energy* **290**, 130174. https://doi.org/10.1016/j.energy.2023.130174 (2024).
34. Zandi-Mehran, N. et al. FFT bifurcation: a tool for spectrum analyzing of dynamical systems. *Appl. Math. Comput.* **422**, 126986. https://doi.org/10.1016/j.amc.2022.126986 (2022).
35. Huang, Q. et al. CrossGNN: Confronting Noisy Multivariate Time Series Via Cross Interaction Refinement, NeurIPS,2023.3.
36. Yang, C., Liu, J., Zhou, K. & Jiang, X. Semisupervised Machine Fault diagnosis fusing unsupervised Graph Contrastive Learning. *IEEE Trans. Industr. Inf.* **19**, 8644–8653. https://doi.org/10.1109/TII.2022.3220847 (2023).
37. Gao, Y. & Yu, D. Intelligent fault diagnosis for rolling bearings based on graph shift regularization with directed graphs. *Adv. Eng. Inform.* **47**, 101253. https://doi.org/10.1016/j.aei.2021.101253 (2021).
38. Zhang, F. et al. A health condition assessment and prediction method of Francis turbine units using heterogeneous signal fusion and graph-driven health benchmark model. *Eng. Appl. Artif. Intell.* **126**, 106974. https://doi.org/10.1016/j.engappai.2023.106974 (2023).
39. Leng, Y. J., Peng, D. & Zhang, H. Integrated energy system evaluation method based on dimensionality reduction and indexes updating with incomplete information. *Energy* **277**, 127552. https://doi.org/10.1016/j.energy.2023.127552 (2023).
40. Zhu, W. et al. Uncertainty quantification of proton-exchange-membrane fuel cells degradation prediction based on bayesian-gated recurrent unit. *eTransportation* **16**, 100230. https://doi.org/10.1016/j.etran.2023.100230 (2023).

41. Wu, H., Xu, J., Wang, J., Long, M., Autoformer & Decomposition transformers with auto-correlation for long-term series forecasting. *Adv. Neural. Inf. Process. Syst.* **34**, 22419–22430. https://doi.org/10.48550/arXiv.2106.13008 (2021).
42. Zhou, H. et al. Informer: beyond efficient transformer for long sequence time-series forecasting. *AAAI* **11106–11115** https://doi.org/10.1609/aaai.v35i12.17325 (2021).
43. Zeng, A., Chen, M., Zhang, L. & Xu, Q. Are transformers effective for time series forecasting? *AAAI*. **11121-11128** https://doi.org/10.1609/aaai.v37i9.26317 (2023).
44. Cai, W., Liang, Y., Liu, X., Feng, J. & Wu, Y. MSGNet: learning multi-scale inter-series correlations for multivariate time series forecasting. *AAAI* **11141–11149** https://doi.org/10.1609/aaai.v38i10.28991 (2024).
45. Xu, J. et al. Study on fuel injection stability improvement in marine low-speed dual-fuel engines. *Appl. Therm. Eng.* **253**, 123729. https://doi.org/10.1016/j.applthermaleng.2024.123729 (2024).
46. Liu, Y. et al. Real-time comprehensive health status assessment of hydropower units based on multi-source heterogeneous uncertainty information. *Measurement* **216**, 112979. https://doi.org/10.1016/j.measurement.2023.112979 (2023).

Acknowledgements

Much of the work presented in this paper was supported by the Corporate and Public Institution Commissioned Scientific Project: Pilot Construction of Automated Pump Station.

Author contributions

Author contributionsPanpan Qiu: Methodology, Formal analysis, and Writing—Original draft. Jianzhuo Yan: Conceptualization, Resources, Writing—Review, Editing, and Funding acquisition. Hongxia Xu: Manuscript revision. Yongchuan Yu: Manuscript revision.

Declarations

Competing interests

The authors declare no competing interests.

Additional information

Correspondence and requests for materials should be addressed to Y.Y.

Reprints and permissions information is available at www.nature.com/reprints.

Publisher's note Springer Nature remains neutral with regard to jurisdictional claims in published maps and institutional affiliations.